nature portfolio

https://doi.org/10.1038/s41586-025-09843-w

Supplementary information

Palaeometabolomes yield biological and ecological profiles at early human sites

In the format provided by the authors and unedited

Palaeometabolomes yield biologic and ecologic profiles at early human sites

Timothy G. Bromage[1,2,3*], Christiane Denys[4], Christopher Lawrence De Jesus[5], Hediye Erdjument-Bromage[5], Ottmar Kullmer[3,6], Oliver Sandrock[7], Friedemann Schrenk[3,6], Marc D. McKee[8], Natalie Reznikov[9], Gail M. Ashley[10], Bin Hu[1], Sher B. Poudel[11], Antoine Souron[12], Daniel J. Buss[8], Eran Ittah[9], Jülide Kubat[3], Sasan Rabieh[13], Shoshana Yakar[1], Thomas A. Neubert[5]

[1] Department of Molecular Pathobiology, New York University College of Dentistry, New York, USA

[2] Department of Anthropology, New York University, New York, USA

[3] Division of Paleoanthropology, Senckenberg Research Institute and Natural History Museum, Frankfurt a. M., Germany

[4] Institute of Systematics and Evolution of Biodiversity, National Museum of Natural History, Paris, France

[5] Department of Neuroscience and Physiology and Neuroscience Institute, NYU Grossman School of Medicine, New York, NY, USA

[6] Institute of Ecology, Evolution and Diversity, Goethe University, Frankfurt a. M., Germany

[7] Earth and Life History, Hessisches Landesmuseum Darmstadt, Darmstadt, Germany

[8] Faculty of Dental Medicine and Oral Health Sciences, and Department of Anatomy and Cell Biology, McGill University, Montreal, Canada

[9] Department of Bioengineering, McGill University, Montreal, Canada

[10] Department of Earth and Planetary Sciences, Rutgers, the State University of New Jersey, New Brunswick, New Jersey, USA

[11] Eurofins Lancaster Laboratories PSS, Lancaster, USA

[12] Univ. Bordeaux, CNRS, Ministère de la Culture, PACEA, UMR 5199, F-33600 Pessac, France

[13] Department of Dental Hygiene & Dental Assisting, New York University Dentistry, New York, USA

Supplementary Information

Guide to SI Figures

SI Figure 1. Polarised light image of specimen HCRP-RC-11 883. *Elephas recki shungurensis*, Bed Unit 3A-2, Level RC 11; a. Dentine illustrating areas of oxidative damage (yellow-brown) and some brightness (grey) associated with collagen. Polarisation colors are presented in the crystalline matrix attached to the lower portion of the fragment. FW=7.806 mm. b. Image of diagenetically affected dentine. FW=0.324 mm.

SI Figure 2. Polarised light image of specimen TF12 Lime Dumps. Bovidae, Bed I; a. Birefringent brightness is attributed to collagen in the bone fragment (left) and accreted sedimentary matrix (right). FW=7.01 mm; b. Detail of bone and diagenetically altered osteocyte lacunae. FW=0.324 mm.

SI Figure 3. BSE-SEM image of specimen HCRP-RC-11 883. *Elephas recki shungurensis*, Bed Unit 3A-2, Level RC 11; a. Macroscopic view of the dentine fragment (left) and crystalline matrix (right). Note that the yellow-brown hues in SI Figure 1a are not associated with variability in mineralization density. FW=8.022 mm; b. Detail of dentine tubules, high mineralisation density peri-tubular dentine, and mineralization density variation in the intertubular matrix, with a CaCO3 crystalline matrix filled crack at left. FW=0.25 mm.

SI Figure 4. BSE-SEM image of specimen TF12 Lime Dumps. Bovidae, Bed I; a. Macroscopic view of the bone fragment (left) and accreted sedimentary matrix (right). FW=6.764 mm; b. Detail of bone illustrating a vascular canal and its surrounding osteonal bone and osteocyte lacunae their associated canaliculi. FW=0.25 mm.

SI Figure 5. Proteomics of the Olduvai Gorge rodent fossils. Gene ontology and pathways of collagen matrices. Color codes in the table relate to the gene network above.

SI Figure 6. Proteomics of the Olduvai Gorge rodent fossils. Gene ontology of collagen matrices.

SI Figure 7. Proteomics of the Olduvai Gorge rodent fossils. Gene cooccurrence illustrating a potential association with those of *Trypanosoma brucei* (above the blue line) particularly of the Olduvai Gorge Fossil Xi (cf. SI Table 8k).

SI Figure 8. Principal Component Analysis (PCA) of the study sample metabolomes. A 2D PCA plot showed clear clustering of samples by origin: fossil, soil, and modern. This zoomed-out plot is only useful or understanding that the modern heterogenous mouse (UM-HET 3) and the Olduvai Gorge Bed II *Kolpochoerus majus* samples are at extreme principal component positions.

SI Figure 9. Principal Component Analysis (PCA) of the study sample metabolomes. Zoomed-in view of SI Figure 20 with outliers removed.

SI Figure 10. Hierarchical Clustering Heatmap of the study sample metabolomes. A z-score normalized heatmap using the top 100 most variable metabolites revealed structured clustering across sample types. We selected the top 25 metabolites to enhance label readability, ensuring visual clarity for readers.

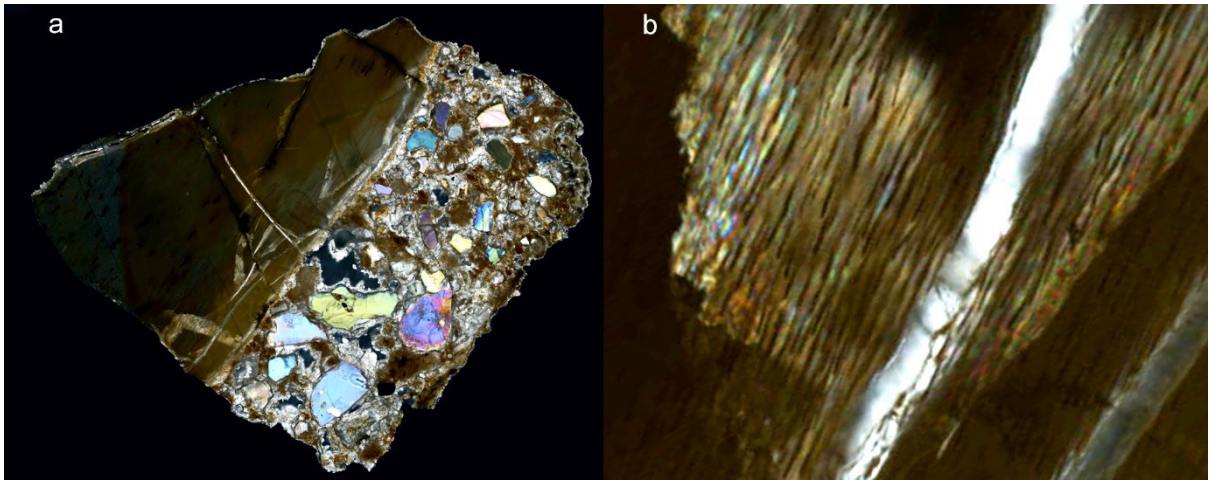

SI Figure 1. Polarised light image of specimen HCRP-RC-11 883. *Elephas recki shungurensis*, Bed Unit 3A-2, Level RC 11; a. Dentine illustrating areas of oxidative damage (yellow-brown) and some brightness (grey) associated with collagen. Polarisation colors are presented in the crystalline matrix attached to the lower portion of the fragment. FW=7.806 mm; b. Image of diagenetically affected dentine. FW=0.324 mm.

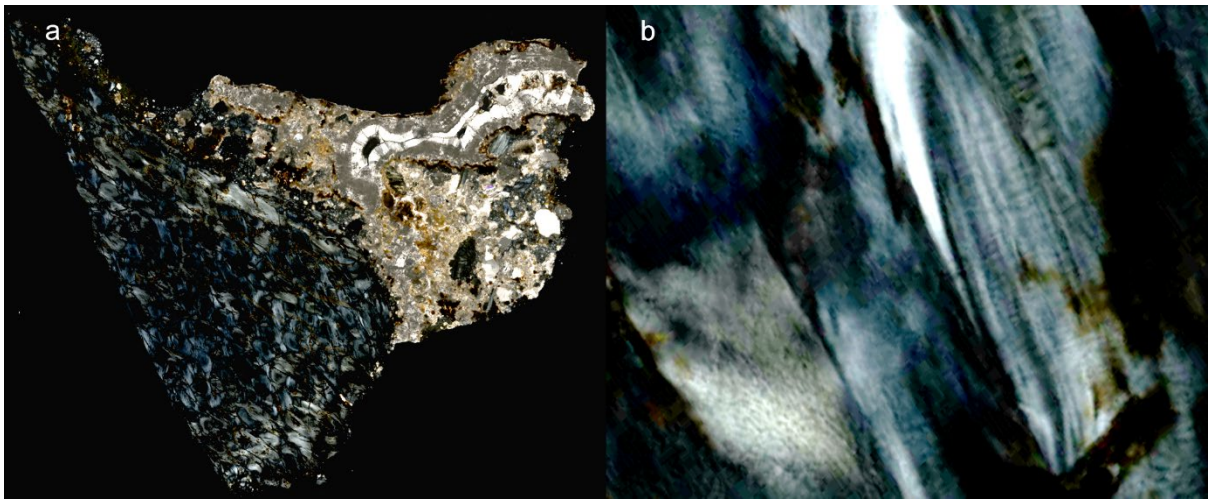

SI Figure 2. Polarised light image of specimen TF12 Lime Dumps. Bovidae, Bed I; a. Birefringent brightness is attributed to collagen in the bone fragment (left) and accreted sedimentary matrix (right). FW=7.01 mm; b. Detail of bone and diagenetically altered osteocyte lacunae. FW=0.324 mm.

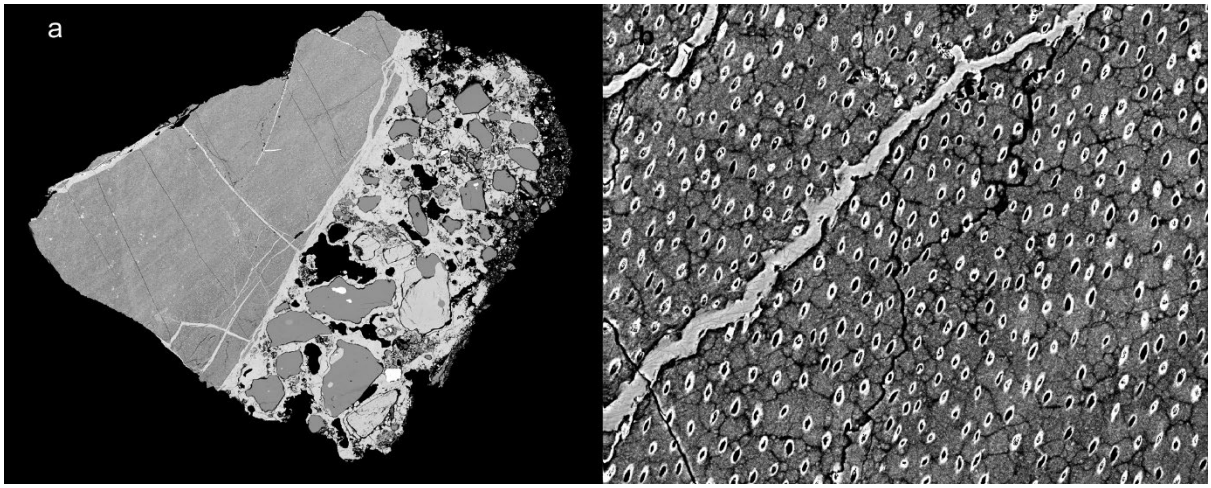

SI Figure 3. BSE-SEM image of specimen HCRP-RC-11 883. *Elephas recki shungurensis*, Bed Unit 3A-2, Level RC 11; a. Macroscopic view of the dentine fragment (left) and crystalline matrix (right). FW=8.022 mm; b. Detail of dentine tubules, high mineralisation density peri-tubular dentine, and mineralization density variation in the intertubular matrix, with a CaCO3 crystalline matrix-filled cracks at left. FW=0.25 mm.

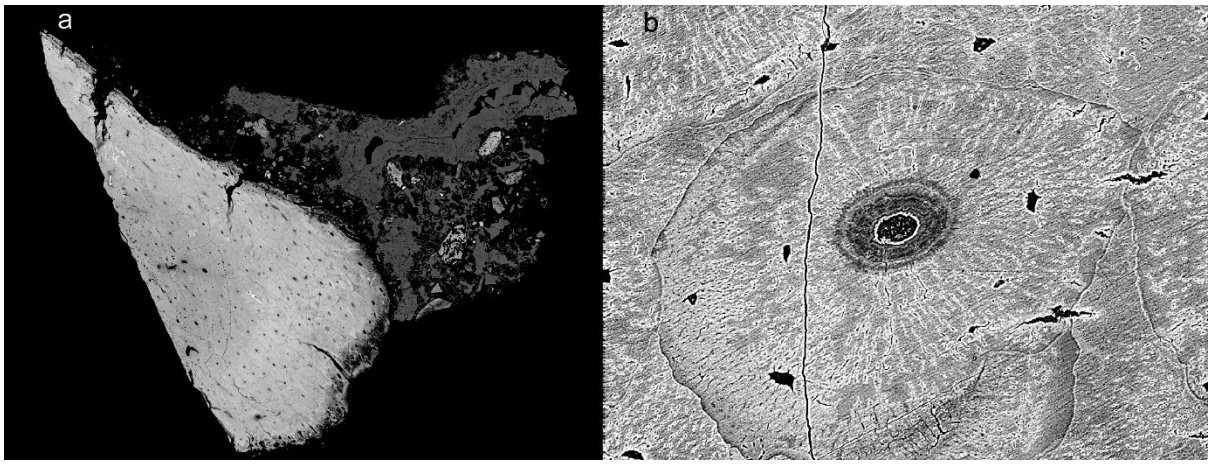

SI Figure 4. BSE-SEM image of specimen TF12 Lime Dumps. Bovidae, Bed I; a. Macroscopic view of the bone fragment (left) and accreted sedimentary matrix (right). FW=6.764 mm; b. Detail of bone illustrating a vascular canal and its surrounding osteonal bone and osteocyte lacunae their associated canaliculi. FW=0.25 mm.

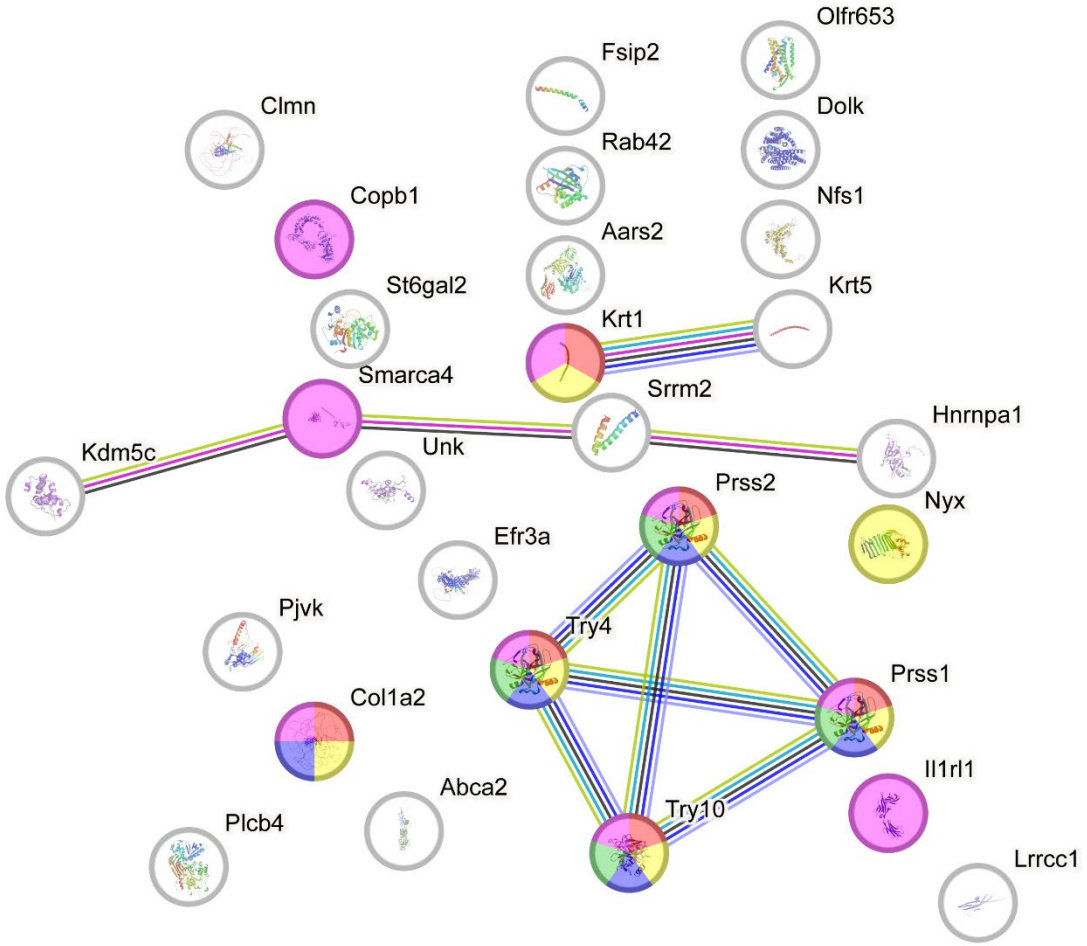

	Cellular Component (Gene Ontology)				
GO-term	description	count in network	strength	signal	false discovery rate
GO:0062023	Collagen-containing extracellular matrix	6 of 397	1.07	0.66	0.0078
GO:0031012	Extracellular matrix	7 of 528	1.01	0.64	0.0078
	Reactome Pathways				
pathway	description	count in network	strength	signal	false discovery rate
MMU-1442490	Collagen degradation	5 of 55	1.85	1.75	2.06e-05
MMU-1592389	Activation of Matrix Metalloproteinases	4 of 35	1.95	1.55	9.59e-05
MMU-168256	Immune System	9 of 1615	0.64	0.4	0.0237

SI Figure 5. Proteomics of the Olduvai Gorge rodent fossils. Gene ontology and pathways of collagen matrices. Color codes in the table relate to the gene network above.

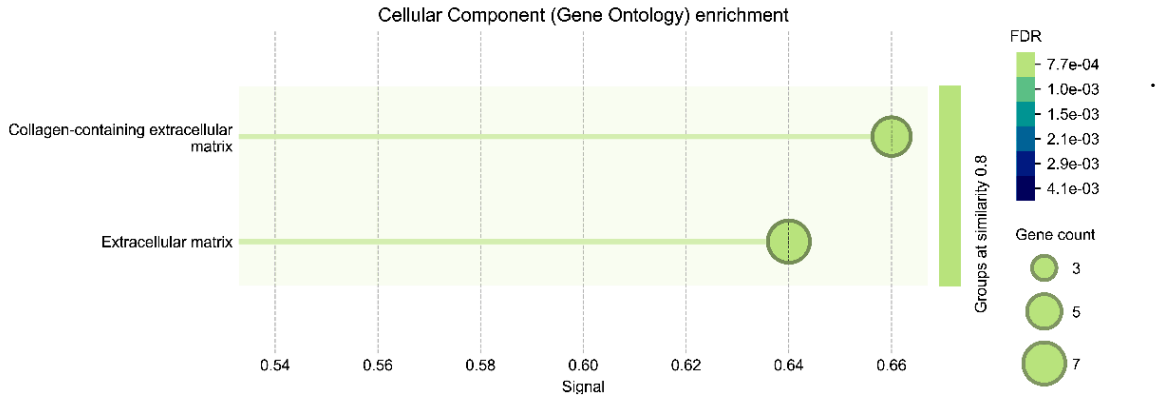

SI Figure 6. Proteomics of the Olduvai Gorge rodent fossils. Gene ontology of collagen matrices.

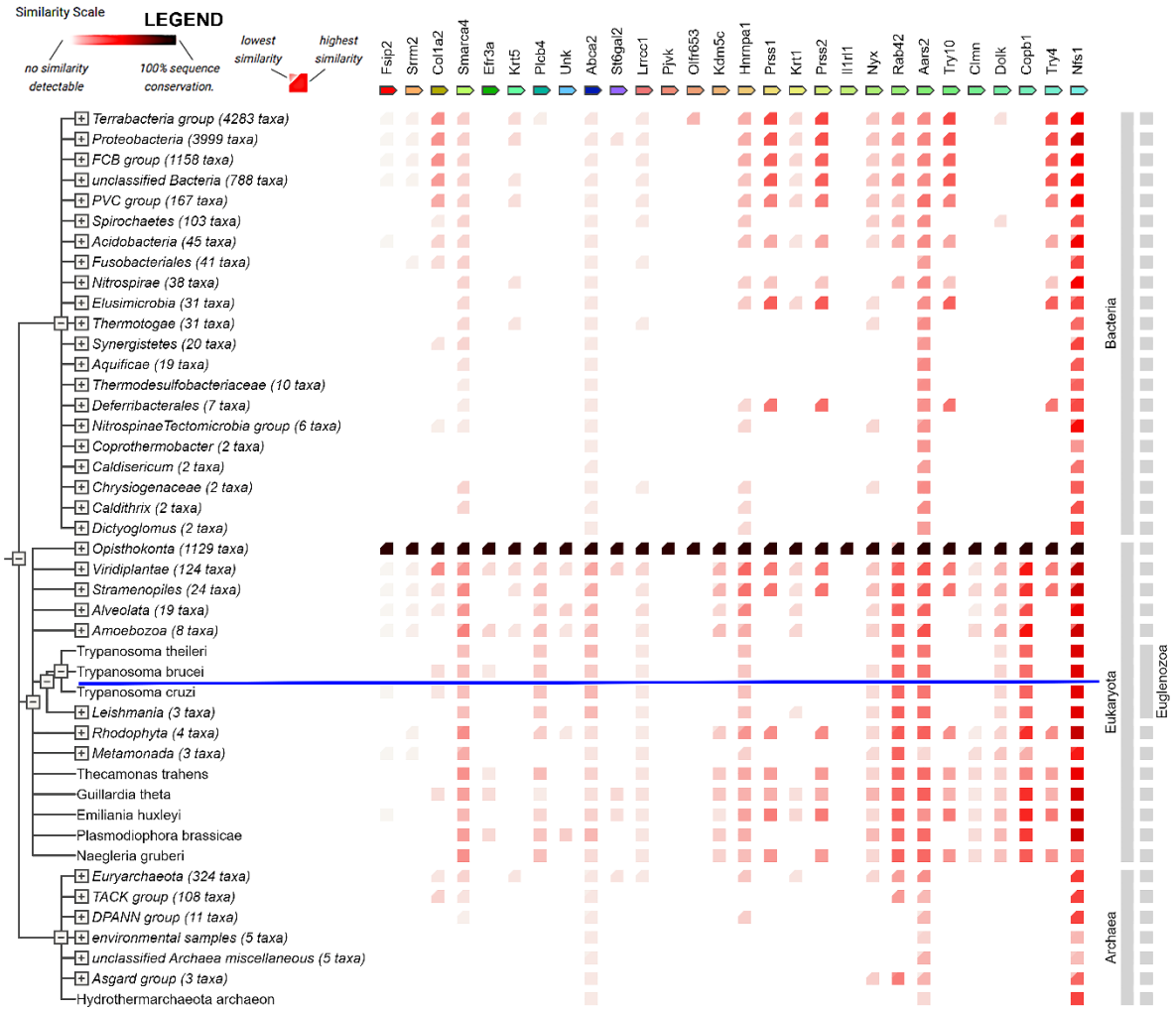

SI Figure 7. Proteomics of the Olduvai Gorge rodent fossils. Gene cooccurrence illustrating a potential association with those of *Trypanosoma brucei* (above the blue line) particularly of the Olduvai Gorge Fossil Xi (cf. SI Table 8k).

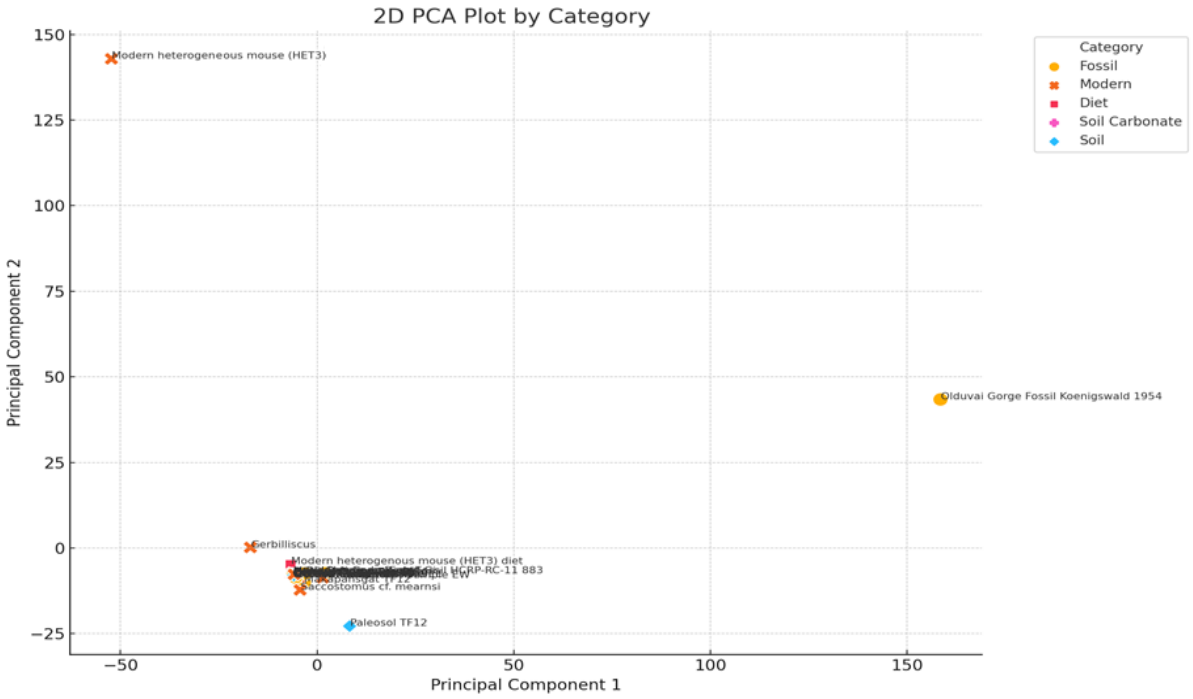

SI Figure 8. Principal Component Analysis (PCA) of the study sample metabolomes. A 2D PCA plot showed clear clustering of samples by origin: fossil, soil, and modern. This zoomed-out plot is only useful or understanding that the modern heterogenous mouse (UM-HET 3) and the Olduvai Gorge Bed II *Kolpochoerus majus* samples are at extreme principal component positions.

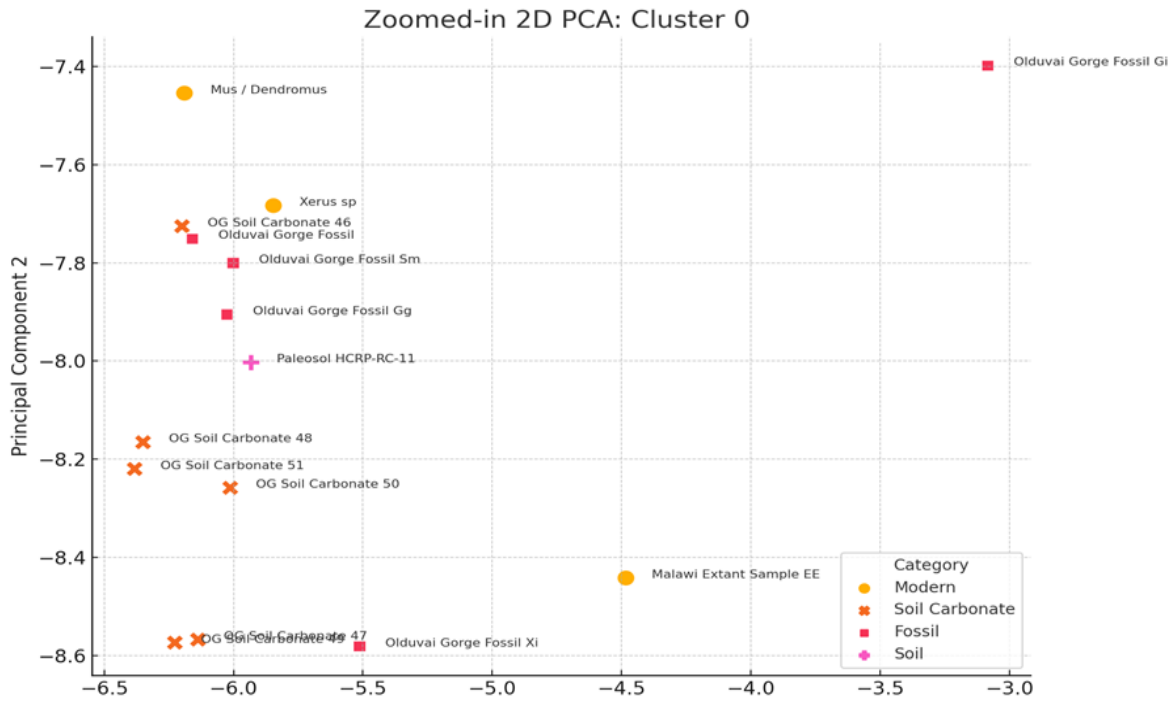

SI Figure 9. Principal Component Analysis (PCA) of the study sample metabolomes. Zoomed-in view of SI Figure 20 with outliers removed.

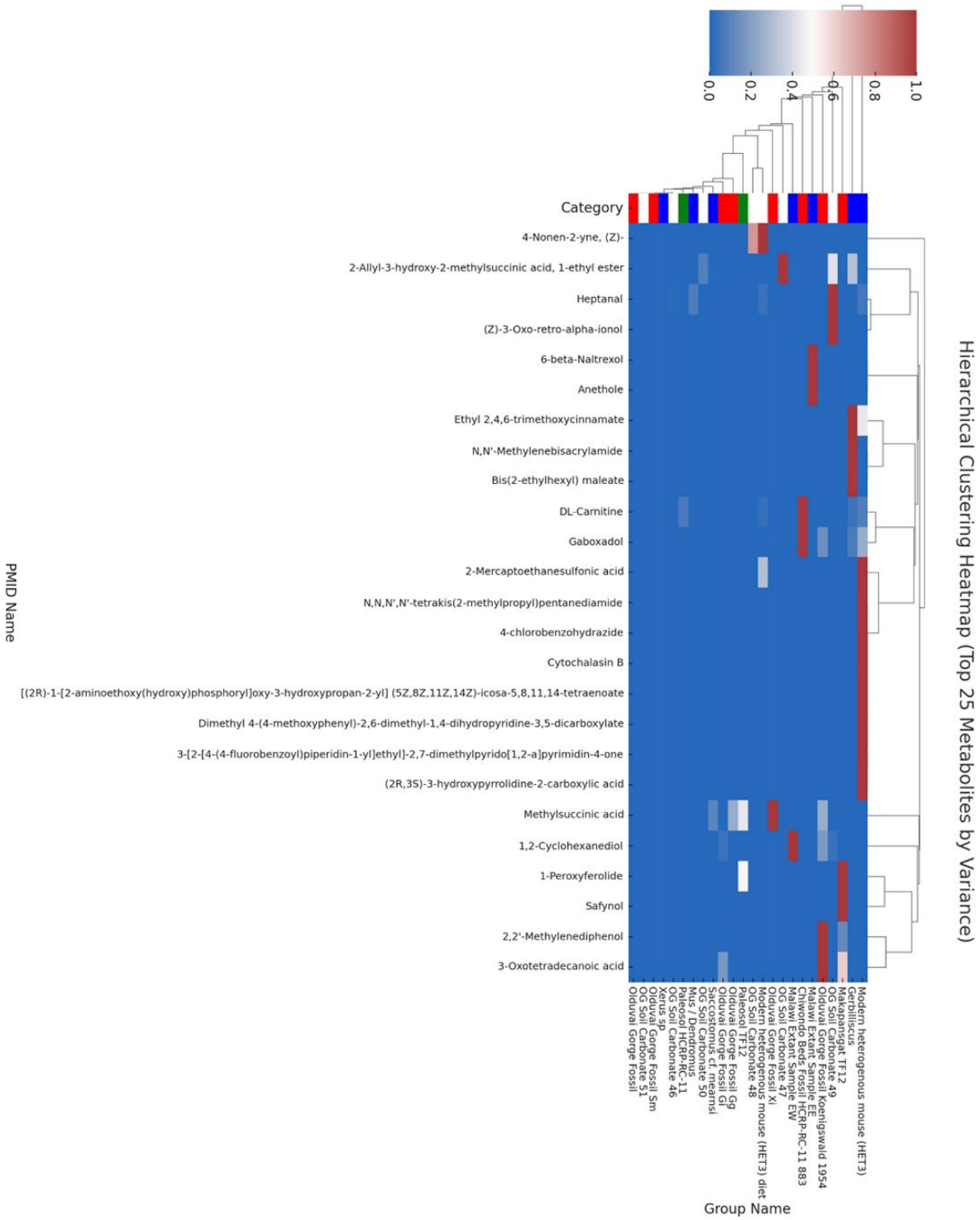

SI Figure 10. Hierarchical Clustering Heatmap of the study sample metabolomes. A z-score normalized heatmap using the top 100 most variable metabolites revealed structured clustering across sample types. We selected the top 25 metabolites to enhance label readability, ensuring visual clarity for readers.